*Desalination and Water Treatment*
www.deswater.com

doi: 10.1080/19443994.2016.1189245

57 (2016) 26886–26898
November

Taylor & Francis
Taylor & Francis Group

# Recovery and development of correlations for heat and mass transfer in vacuum membrane distillation for desalination

Sushant Upadhyaya*, Kailash Singh, S.P. Chaurasia, Rajeev Kumar Dohare, Madhu Agarwal

*Department of Chemical Engineering, Malaviya National Institute of Technology, Jaipur, India, Tel. +91 9549654173; Fax: +91 141 2713486; email: supadhyay.chem@mnit.ac.in (S. Upadhyaya)*

Received 1 August 2015; Accepted 9 April 2016

ABSTRACT

This study evaluates the recovery of pure water by vacuum membrane distillation (VMD). The VMD process has been experimentally studied using a polytetrafluroethylene (PTFE) membrane for aqueous sodium chloride solution containing salt concentration of 20,000 ppm and permeate pressure of 7 kPa. The percentage recovery was observed to increase with time of operation and in 183 h, it became 86%. A mathematical model for recovery has also been developed and validated with experimental data. Heat transfer and mass transfer correlations have been developed for the range of feed flow rate of 0.5–2 lpm and feed bulk temperature of 40–60˚C. The effect of feed salt concentration and membrane fouling was also studied on permeate flux. Permeate flux was found to decrease by 15 and 10% at 55 and 60˚C, respectively, on increasing feed salt concentration from 5 to 40 g/l. The permeate flux was observed to decrease by 8% from 26.1 to 24 $kg/m^2$ h after continuous operation of 180 h at 60˚C and 20,000 ppm feed salt concentration due to fouling. However, after washing the membrane with water, the flux regained up to 25.7 $kg/m^2$ h. The fouling was confirmed in the study of membrane morphology using SEM images.

*Keywords:* Vacuum membrane distillation; Recovery; Heat and mass transfer correlation; PTFE; Modeling; Desalination

## 1. Introduction

Vacuum membrane distillation (VMD) is a thermally driven process, in which only vapor molecules are transported through porous hydrophobic membranes; the downstream pressure during the process is kept lower than the equilibrium vapor pressure of volatile components to be separated from the feed solution [1,2]. In a VMD configuration, vacuum is applied on the permeate side of the module by a vacuum pump. The applied vacuum pressure is lower than the saturation pressure of volatile components to be separated from the feed solution. The liquid feed to be treated by VMD must be in direct contact with one side of the membrane and should not penetrate the dry pores of the membranes. Liquid/vapor interface is formed at the entrances of the membrane pores. The driving force is the transmembrane vapor pressure difference that may be maintained in the permeate

*Corresponding author.

*Presented at Trombay Symposium on Desalination and Water Reuse, Mumbai, India, 22–23 January 2015*

side of the membrane [3]. VMD is an emerging technology for desalination and is distinct from the other membrane separation processes in terms of driving force as vapor pressure instead of total pressure.

An increasing number of areas on our planet will suffer more in the near future because of rapid depletion of ground water and surface water [4]. VMD has been applied for water reuse, water desalination, environmental waste clean-up, food processing, milk and juice concentration, biomedical applications such as water removal from blood, and treatment of protein solutions. Lower operating systems' temperatures has also made VMD attractive in the food industry where concentrated fruit juices can be prepared with better flavor and color [5] Since VMD is a thermally driven process, operating pressure is generally of the order of zero to a few kPa, relatively low as compared to pressure-driven processes such as reverse osmosis. VMD and conventional distillation processes work on the principle of vapor–liquid equilibrium for separation; both operations involve the latent heat of vaporization to create vapor phase. Despite this, the main difference between these two operations is that in conventional distillation, the liquid solution is required to be heated up to the bubble point, whereas it is not required in the case of VMD. VMD performs well with the feed temperature lower than its boiling point. In addition to it, the components to be separated can form an azeotropic mixture and have close boiling points. Hence, VMD belongs to a special class of distillation process [6].

Recently, numerous mathematical models have been developed for VMD. Mainly, these models [1,7–24] have been used for the prediction of permeate flux and estimate the sensitivity of various parameters such as feed flow rate, feed bulk inlet temperature, feed concentration, permeate pressure, pore diameter, membrane thickness, and membrane porosity. Mathematical models on membrane distillation have been reviewed by Lawson and Lloyd [24]. Several researchers assumed Knudsen flow for gas permeation through membrane as the basis in their models [9,24–29]. Some other authors took into consideration the combination of Knudsen–Poiseuille flow for their models to estimate the VMD flux [21,24,30]. Many attempts were made in developing the theoretical model for better understanding of VMD process without due attention of characterization of VMD membrane before and after utilization for explaining the fouling effect [31,32].

Numerous heat transfer correlations were developed for VMD to apprehend the effect of heat transfer coefficient (HTC) on feed bulk inlet temperature by many investigators [9,15,21,24,33], but no systematic study has been reported to develop the mass transfer correlation for VMD process. The HTC at boundary layer is generally determined by correlations for heat exchangers, but these may not be appropriate in determining the HTC at boundary layer in case of VMD since these well-known correlations for heat exchanger are based on non-porous and rigid heat exchanger, while the membrane used in VMD is porous and non-rigid. Due to this difference, the correlations for heat exchanger and VMD are not identical. Moreover, it is known that the VMD process is influenced by the combination of mass, heat, and momentum transport. Hence, in the present study, various experimental runs were conducted in VMD at various feed flow rates, feed bulk inlet temperatures, etc. by ascertaining all the considerations like porous, non-rigid membrane, temperature polarization, and coupling of heat and mass transfer phenomena to develop heat transfer and mass transfer correlations.

Recovery is defined as the fraction of feed flow through the membrane and ranges from 0 to 1. It is a parameter of economic importance. Commercially, membrane processes are designed with a recovery value as high as possible; however, high recovery influences the membrane process performance in due course of time.

So far, no paper has been found that discusses a theoretical mathematical model for recovery and effect of feed temperature on recovery for desalination by VMD. In the present paper, experimental study has been performed on VMD using a polytetrafluoroethylene (PTFE) membrane. A theoretical model for recovery calculation has been developed, which has been validated with the experimental data. The permeate flux at various feed temperatures has been computed theoretically to determine the recovery. The correlations for heat transfer and mass transfer coefficients have been developed. The effect of fouling on permeate flux has also been studied. The fouling on membrane has been corroborated with energy dispersive spectroscopy (EDS) data of used membrane. The pore size distribution of PTFE membrane has also been measured to confirm the blocking of pores after utilization.

## 2. Mathematical modeling for recovery in VMD

A schematic diagram for recovery calculation is depicted in Fig. 1.

Assuming density as constant, overall material balance in the membrane module is:

$$Q_F = Q_R + Q_P \tag{1}$$

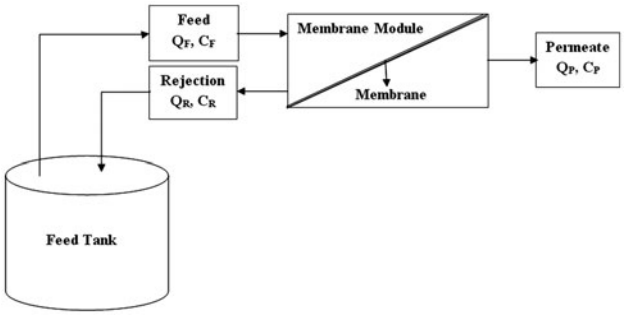


Fig. 1. A schematic diagram for recovery calculation.

Salt material balance in feed tank is:

$$\frac{d(C_F V)}{dt} = Q_R C_R - Q_F C_F \tag{2}$$

$$C_F \frac{dV}{dt} + V \frac{dC_F}{dt} = C_R Q_R - Q_F C_F \tag{3}$$

Overall material balance in feed tank is:

$$\frac{dV}{dt} = Q_R - Q_F \tag{4}$$

Substituting Eq. (4) in Eq. (3), we get:

$$C_F(Q_R - Q_F) + V \frac{dC_F}{dt} = C_R Q_R - Q_F C_F \tag{5}$$

$$\Rightarrow V \frac{dC_F}{dt} = C_R Q_R - Q_F C_F - C_F Q_R + Q_F C_F \tag{6}$$

$$\Rightarrow \frac{dC_F}{dt} = \frac{(C_R - C_F)Q_R}{V} \tag{7}$$

Applying salt material balance in membrane module:

$$\frac{d(C_R V_m)}{dt} = Q_F C_F - C_R Q_R - C_P Q_P \tag{8}$$

Eq. (8) can be rewritten by equating $C_P$ to zero as:

$$\frac{d(C_R V_m)}{dt} = Q_F C_F - C_R Q_R \tag{9}$$

$$\Rightarrow \frac{d(C_R)}{dt} = \frac{Q_F C_F - C_R Q_R}{V_m} \tag{10}$$

The permeate flux (permeate flow rate per unit area of membrane) can be calculated using the following equation [23]:

$$N = \frac{\varepsilon}{\tau\delta RT_{fm}} \left\{ \frac{1 - y_A}{D_{AB}} + \frac{3}{4d} \sqrt{\frac{2\pi M}{RT_{fm}}} \right\}^{-1} (P_{fm} - P_{pm}) + \frac{\varepsilon r^2}{\tau\delta} \frac{P_{fm} M}{8\eta RT_{fm}} (P_{fm} - P_{pm}) \tag{11}$$

where $P_{fm}$ and $P_{pm}$ are partial pressures in feed side and permeate pressure of water, respectively. The porosity of PTFE membrane $\varepsilon$ was taken as 0.70. Thickness of the membrane $\delta$ was 175 microns, tortuosity $\tau$ was 1.6, $T_{fm}$ is the feed side membrane's surface temperature, $D_{AB}$ is the diffusion coefficient, $y_A$ is the mole fraction of water vapor, membrane pore size $d$ (=2$r$) is 0.22 μm, $M$ is the molecular weight of water, and $\eta$ is the viscosity of water vapor (temperature dependent).

The relationship between $Q_P$ and $N$ is as follows:

$$Q_P = \frac{NM\pi D^2}{4\rho} \tag{12}$$

where $D$ is the effective membrane diameter (52 mm) and $\rho$ is the water density.

The value of permeate volumetric flow rate $Q_P$ was calculated using Eq. (12) at various feed inlet temperatures (45, 50, 55, and 60°C). Further, model Eqs. (4), (7), and (10) were simulated in MATLAB by a writing code in M-file using ode15s.

## 3. Experimental

A lab-scale VMD setup was used in the study. The schematic diagram of the experimental setup is shown in the Fig. 2. A flat sheet hydrophobic micro porous PTFE membrane (porosity 70%) with an effective

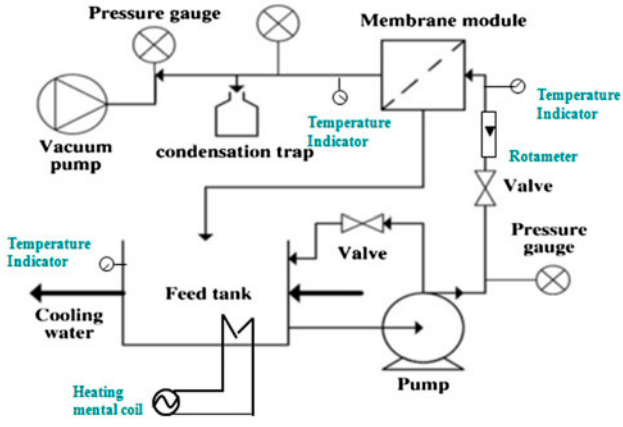


Fig. 2. A schematic diagram of VMD setup.

diameter of 52 mm, pore diameter 0.22 micron, and membrane thickness 175 micron was used for the experiments. The aqueous feed solution of 20 g/l NaCl was prepared and heated to the required temperature using a heating apparatus equipped with a temperature controller at base of the feed tank. The feed solution was then pumped from the feed tank by a feed pump (0.37/0.50 HP of Crompton make) to the membrane unit. The feed was circulated through the membrane module. The feed flow rate was monitored using rotameter installed on the membrane unit. The temperature of both fluids of inlet and outlet was monitored using digital thermometers. A vacuum pump (FRACOVAC make) was installed at the base to create the required vacuum on the permeate side by which the partial pressure difference across the membrane was maintained.

A condenser unit was used at the permeate side to condense the vapor coming from the membrane unit. A cold water reservoir was housed in the setup to supply cold water to the condenser unit. A permeate receiver was used to collect the water, which comes from the condenser. A pressure gauge was used to measure and maintain the vacuum created. Electrical conductivity of the distillate permeate was measured using a multi-ion meter (Thermo Scientific Orion USA make). The specifications and makeup of the various instruments used in the setup are shown in Table 1.

## 4. Results and discussion

### 4.1. Water recovery

The water recovery through VMD was calculated using the developed model equations. The average permeate flow rate was estimated by carrying out VMD experiment and collecting the permeate over a definite period of time which was obtained to be 0.0471 kg/h, assumed to be constant for the whole time of operation. The retentate was recycled into the feed tank. The feed flow rate, feed inlet temperature, and permeate pressure were kept at 1 lpm, 60˚C, and 7 kPa, respectively. The initial volume of water in the feed tank was 10 L with the concentration of 20,000 ppm of NaCl. The recovery was calculated as shown in Fig. 3. It was assumed that the maximum feed concentration can go up to 45,000 ppm, beyond which the tank is refilled with fresh feed. The water recovery increased with time and it was 86% at 183 h. The recovery time is high due to low effective area of the membrane used in the setup, which was 0.00212 $m^2$. However, on using the membrane of effective area of 1 $m^2$, the recovery time reduced to $183 \times 0.00212/1 = 0.38796$ h or 23.2 min. It can be seen from Fig. 3 that the developed model for recovery is in good agreement with experimental recovery.

The transient salt concentration in feed tank and recovery was also calculated using the model equations at temperatures 45, 50, 55, and 60˚C as shown in Figs. 4 and 5, respectively, at feed flow rate of 1 lpm and permeate pressure of 7 kPa. It is clear from Fig. 4 that salt concentration in the tank goes on increasing and becomes 22, 27, 34, and 55 $kg/m^3$ in 200 h at 45, 50, 55, and 60˚C, respectively. It can also be observed that at high temperature, such as 60˚C, the salt rejection rate increases exponentially, suggesting that higher temperature favors the salt rejection rate.

Fig. 5 illustrates the percent recovery as calculated by model equations at various feed inlet temperatures: 45, 50, 55, and 60˚C. It can be observed that the recovery increases linearly with time and at 200 h, it becomes 16, 39, 64, and 95% at feed inlet temperatures of 45, 50, 55, and 60˚C, respectively.

### 4.2. Heat transfer correlation development

The HTCs on the boundary layers are generally calculated from well-known heat transfer empirical correlations. These correlations are valid only for non-porous and rigid heat exchangers. However, the membranes are porous in nature. Therefore, there is a difference between the mechanisms of heat transfer in membrane distillation systems and in heat exchangers. Moreover, in an MD system, the heat transfer is

Table 1
Specifications and makeup of various instruments used in VMD setup

| Instrument | Specification | Make |
|---|---|---|
| Thermocouple | 0–125˚C with least count of 1˚C | RT 100 |
| Rotameter | Range 0–2 lpm, Accuracy 99.16% | Star flow India |
| Pressure gauge | 0–2.5 $kg_f/m^2$ | Gluck |
| Vacuum gauage | 0 to −760 mm Hg with least count of 20 mm Hg | Guru India |
| Multi-ion meter | Advanced microprocessor based total electrochemistry benchtop meter V star 93 | Thermo Scientific Orion USA make |

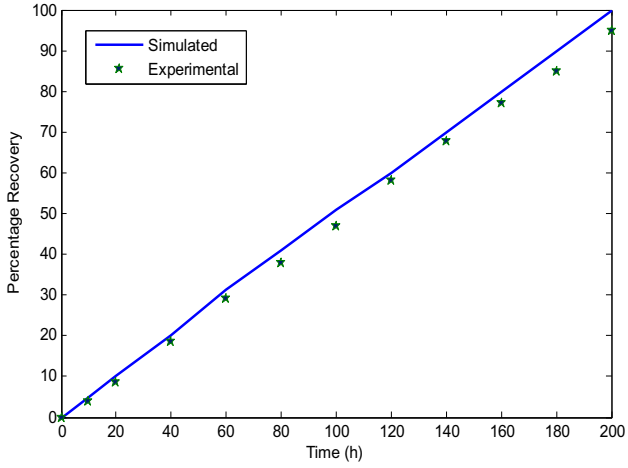


Fig. 3. Percent recovery in VMD with time.

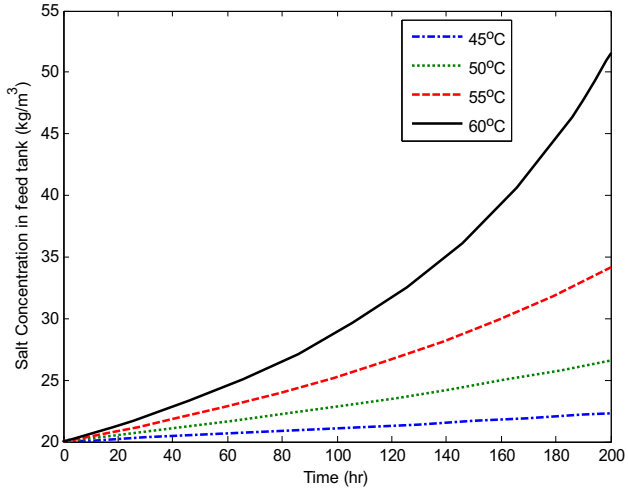


Fig. 4. Effect of feed side inlet temperature on salt concentration in feed tank.

coupled with mass transfer [24]. In this work, VMD heat transfer phenomenon was studied using a test cell module consisting of PTFE flat sheet membrane. The temperature polarization effect and the mechanisms of heat and mass transfer through the system have been considered. The experimental heat transfer correlation was obtained in terms of Nusselt, Reynolds, and Prandtl numbers.

The heat energy needed for the water to vaporize into the membrane pores is provided by heat transfer through the boundary layer at the feed side. The heat flux is given by:

$$q_f = h_f(t_f - t_{fm}) \tag{13}$$

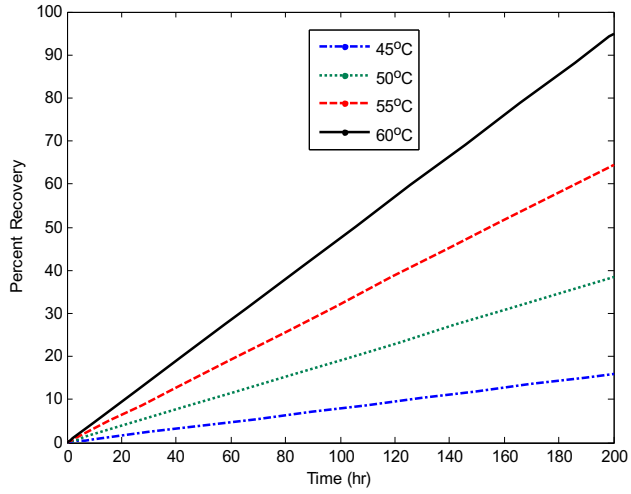


Fig. 5. Effect of feed side inlet temperature on theoretical recovery.

Assuming the contribution of both evaporation and conduction, the total heat flux transferred through the membrane is:

$$q_m = N\Delta H + h_m(t_{fm} - t_{pm}) \tag{14}$$

where $h_m = \frac{(1-\varepsilon)\lambda_s + \varepsilon\lambda_g}{\delta}$, $\lambda_s$ (=0.28 W/m °C) and $\lambda_g$ (=0.021 W/m °C) are thermal conductivities of PTFE membrane material and water vapor in the pores, respectively [22]. The feed side HTC $h_f$ can be calculated by equating Eqs. (13) and (14). In the above calculations, the values of $N$ were taken from experiments. The values of $h_f$ were calculated at various feed temperatures and feed flow rates as shown in Fig. 6. It is observed that the HTC increases as the feed flow rate and feed bulk inlet temperature increase. This may be due to the fact that increasing feed flow rate lowers the salt concentration deposition (reduction in concentration polarization effect) on the membrane, which in turn increases the vapor pressure causing higher permeate flux. Moreover, higher feed bulk temperature also causes increase in vapor pressure on the membrane surface and hence the driving force increases leading to higher permeate flux. Also, the temperature polarization effect decreases on increasing the feed bulk temperature as fluid viscosity decreases and therefore thermal boundary layer thickness decreases, thereby increasing the HTC.

The following empirical correlation was fitted using nonlinear regression, which gives the optimum values of the constants $a$, $b$, and $c$ by minimizing the error between experimental and calculated values using Newton's method. It is found that there is a

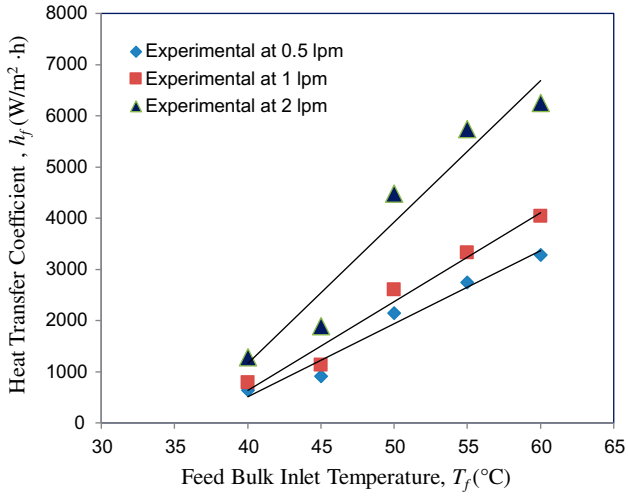


Fig. 6. Effect of feed bulk temperature and feed flow rate on HTC.

following relationship between the HTC and feed bulk inlet temperature:

$$\text{At } 0.5\,\text{lpm}\; h_f = 142.52\,T_f - 5185.6 \tag{15}$$

$$\text{At } 1\,\text{lpm}\; h_f = 173.82\,T_f - 6317.2 \tag{16}$$

$$\text{At } 2\,\text{lpm}\; h_f = 276.1\,T_f - 9879.6 \tag{17}$$

The $R^2$ values for the above equations were found to be 0.970, 0.970, and 0.944, respectively.

The Nusselt number, $Nu$, was calculated by $Nu = h_f\, d_e/k$, where $d_e$ is the effective diameter of membrane and $k$ is the thermal conductivity of water. Reynolds number, $Re$, was calculated by $Re = vd_e\rho/\mu$, where $v$ is the approach velocity of water, $\rho$ and $\mu$ are the density and viscosity of liquid water, respectively. The heat transfer correlation was developed using nonlinear regression for varied feed bulk inlet temperatures and feed flow rates.

$$Nu = a\,Re^b\,Pr^c \tag{18}$$

The correlation after fitting the data was found to be as follows:

$$Nu = 0.43\,Re^{0.837}\,Pr^{0.33} \tag{19}$$

The indexes to Reynold's number and Prandtl number are similar to those reported by others [22]. The plot of theoretical and experimental values of $\log(Nu/Pr^{0.33})$ vs. $\log(Re)$ is shown in Fig. 7. It is observed that the theoretical model is in good agreement with the experimental data. The $R^2$ value was found to be 0.971. It can also be concluded from this correlation that the HTC increases on increasing the feed bulk temperature as the fluid viscosity decreases ($h_f \propto \mu^{-0.5}$).

### 4.3. Mass transfer correlation development

The VMD process involves both heat transfer and mass transfer. The mass transfer is due to the flow of vapors through membrane pores. It depends on permeate pressure, feed temperature, and feed flow rate. Therefore, a correlation was developed to estimate the mass transfer coefficient, $k_f$, (in terms of Sherwood number, $Sh$) as a function of the dimensionless numbers, Reynolds number, and Schmidt number, $Sc$, as follows:

$$Sh = a'\,Re^{b'}\,Sc^{c'} \tag{20}$$

where $Sh = k_f d_e/D_{AB}$, and $Sc = \mu/\rho D_{AB}$. The value of mass transfer coefficient ($k_f$) was calculated using Eq. (21) developed as follows:

$$N = k_f\,(C_{fm} - C_{pm})$$

Putting $C_{fm} = P_{fm}M/RT_{avg}$ and $C_{pm} = P_{pm}M/RT_{avg}$, where $T_{avg}$ is the average of $T_{fm}$ and $T_{pm}$.

Therefore

$$k_f = \frac{NRT_{avg}}{M\left(P_{fm} - P_{pm}\right)} \tag{21}$$

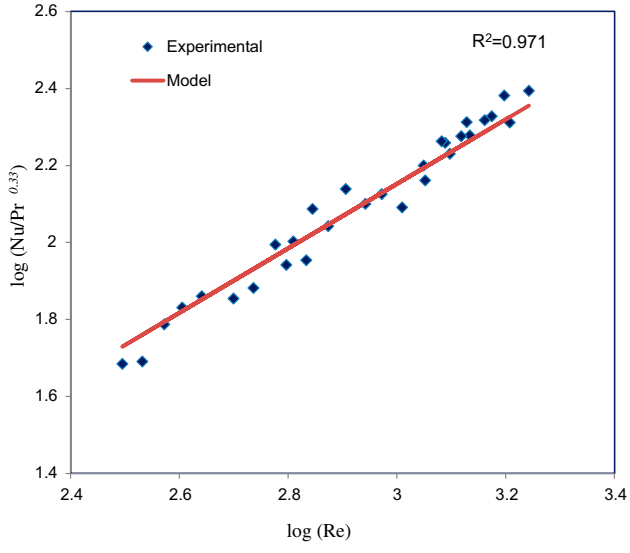


Fig. 7. Heat transfer correlation fitting.

The values of $k_f$ were calculated at various feed temperatures (45–60˚C) and feed flow rates (ranging from 0.5 to 2 lpm). It can also be observed from Fig. 8 that the mass transfer coefficient increases by increasing the feed flow rate and feed bulk inlet temperature. The increment of mass transfer coefficient ($k_f$) with respect to feed flow rate and feed bulk inlet temperature can cause the reduction in concentration and temperature polarization effect. The mass transfer correlation was developed by minimizing the error between the experimental and estimated Sherwood number using Newton's method, given as follows:

$$Sh = 31.79\, Re^{0.46}\, Sc^{0.33} \tag{22}$$

The plot of theoretical and experimental values of log ($Sh/Sc^{0.33}$) vs. log($Re$) is shown in Fig. 9. It is observed that the theoretical model is in good agreement with the experimental data. The $R^2$ value was found to be 0.975.

### 4.4. Effect of feed concentration on permeate flux

The experiments were conducted for various NaCl salt concentrations at feed flow rate of 2 lpm, and permeate pressure of 6 kPa, at different feed bulk temperatures of 55 and 60˚C as shown in Fig. 10. It is observed from this figure that the experimental permeate flux decreases slightly with increase in the feed inlet concentration from 5 to 20 g/l. This decrement was less than 1 and 2% for 55 and 60˚C of feed bulk inlet temperatures, respectively. It shows negligible effect of salt concentration on permeate flux. However, the effect was not negligible at higher feed concentration, i.e. 30–40 g/l. It was observed that the declination of permeate flux was nearly 15 and 10% at 55 and 60˚C feed bulk inlet temperatures, respectively. On increasing the concentration of non-volatile solutes in the form of salt in the feed solution results in the declination of permeate flux due to the decrease of water vapor pressure, as per modified Raoult's Law (The activity coefficient of water for NaCl solution is given by $\gamma = 1–0.5x - 10x^2$, where $x$ is the salt mole fraction), which may affect the driving force for mass transfer. Moreover, at higher salt concentrations, the extra boundary layer is created on the surface of membrane–feed interface. This problem can be minimized by creating turbulence or increasing the feed flow rate for enhancing the VMD performance. Hence, the performance of VMD was different for low salt concentrations and high salt concentrations. However, due to low salt concentrations in ground water, the permeate flux will not change significantly. Sometimes, this reduction of permeate flux at high salt concentrations leads to the crystallization and scaling on membrane surface. But, it was observed that the effect of scaling in water desalination through VMD was not significant. This outcome was also supported by Mohammadi and Safavi [34]. Due to this reason, VMD can be used for desalination of higher salt concentrations as compared to other membrane process like RO without altering a huge drop in production. Since concentration polarization is very large in RO, it ultimately creates reduction in permeate flux to a large extent in RO as compared to the VMD.

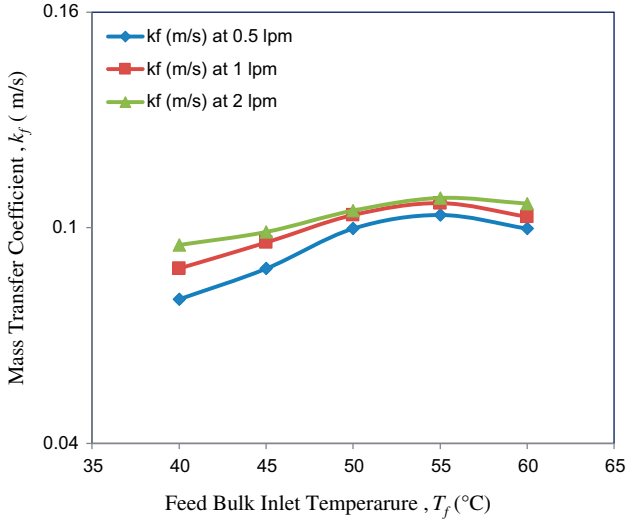


Fig. 8. Effect of feed bulk inlet temperature and feed flow rate on mass transfer coefficient.

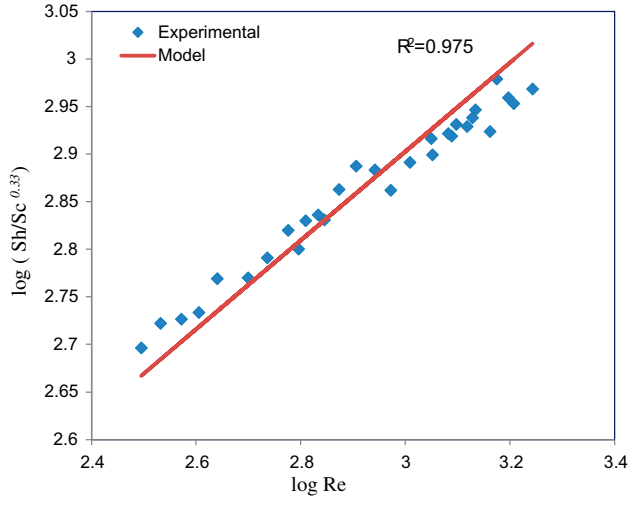


Fig. 9. Mass transfer correlation fitting.

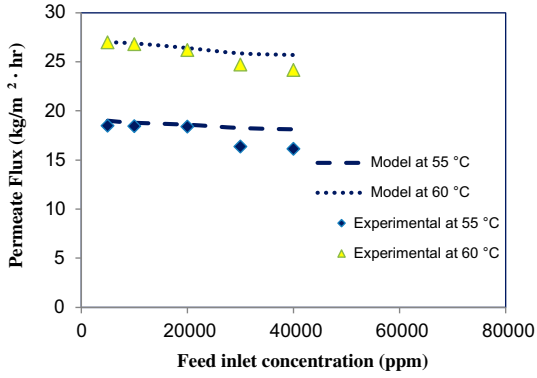


Fig. 10. Effect of feed salt concentration on permeate flux.

Table 2
$R^2$ and MAPE values for effect of feed salt concentration on permeate flux

| Feed bulk temperature (°C) | $R^2$ | MAPE |
|---|---|---|
| 55 | 0.91 | 5.84 |
| 60 | 0.97 | 2.47 |

The mathematical model [23] values were compared with experimental results, and are found to be in good agreement. The $R^2$ and MAPE values are given in Table 2. It can be observed that $R^2$ value corresponding to 55°C is lower than that at 60°C. This deviation from theoretical prediction may be due to increase in concentration polarization effect at low temperature.

Based on the above discussion of the effects of various parameters, the permeate flux is found to be higher at feed temperature of 60°C as compared to that at 55°C.

### 4.5. Effect of membrane fouling on permeate flux

In a continuous operation, the salt concentration of 20 g/l was used as a feed solution for a VMD setup and the transmembrane permeate flux was collected continuously for about 180 h. Fig. 11 shows that there was slight declination of the permeate flux. At 60°C, the permeate flux was 26.1 kg/m$^2$ h and decreased gradually till 180 h at 6 kPa of permeate pressure and 2 lpm of feed flow rate. It was observed that the flux decreased nearly 8% in 180 h, which may be due to the minor scale deposit on the membrane surface. The effective membrane characteristics parameter $\varepsilon/\tau\delta$ decreases on continuous use of membrane due to salt deposition; therefore, the mass flux gets decreased. The PTFE membrane used in the present study was hydrophobic and therefore it has been assumed that there is no wetting of membrane. The fouling was observed over the membrane surface after using for 180 h. Therefore, subsequently, water washing was done and the membrane performance was checked again. It was observed that the flux regained to about 25.7 kg/m$^2$ h under the same process conditions with 99.9% salt rejection.

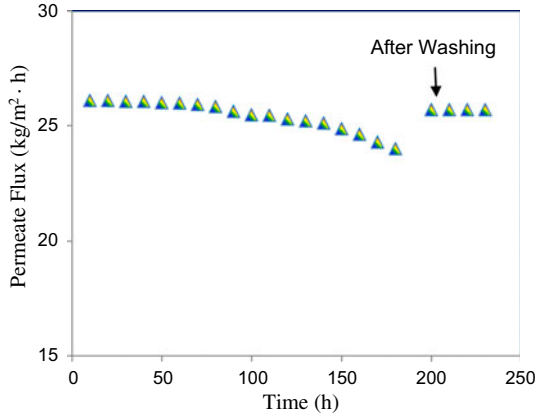


Fig. 11. Variations of permeate flux as a function of operating time.

### 4.6. Comparison of membrane morphology before and after use

The membrane morphology was tested by SEM. The membranes before and after its use in VMD were analyzed. The SEM micrograph of a brand new membrane's morphology is shown in Fig. 12(a). It was observed that the new membrane used in SEM study had pore diameter upto 0.30 μm, whereas the average pore diameter of the membrane was 0.22 μm as per the specifications given by the manufacturer (Millipore). The other characteristics of fresh PTFE membrane are given in Table 1. Large pores of size 10 μm were also observed by other researchers [12,35], despite the average pore size of Accurel PP S6/2 membrane mentioned as 0.22 μm. EDS image is also shown in Fig. 12(b), which indicates the presence of carbon, fluorine, and oxygen atoms, which are the constituents of PTFE membrane.

The PTFE membrane was used continuously under 6 kPa of permeate pressure, feed flow rate of 2 lpm, feed inlet temperature of 60°C, and feed salt concentration of 20,000 ppm for 180-h run time. The SEM micrograph of this membrane is shown in Fig. 13(a). It is seen that there is little fouling over the membrane surface. Therefore, little reduction in permeate flux was observed after 180 h of continuous use of membrane. The flux was almost found to regain its original

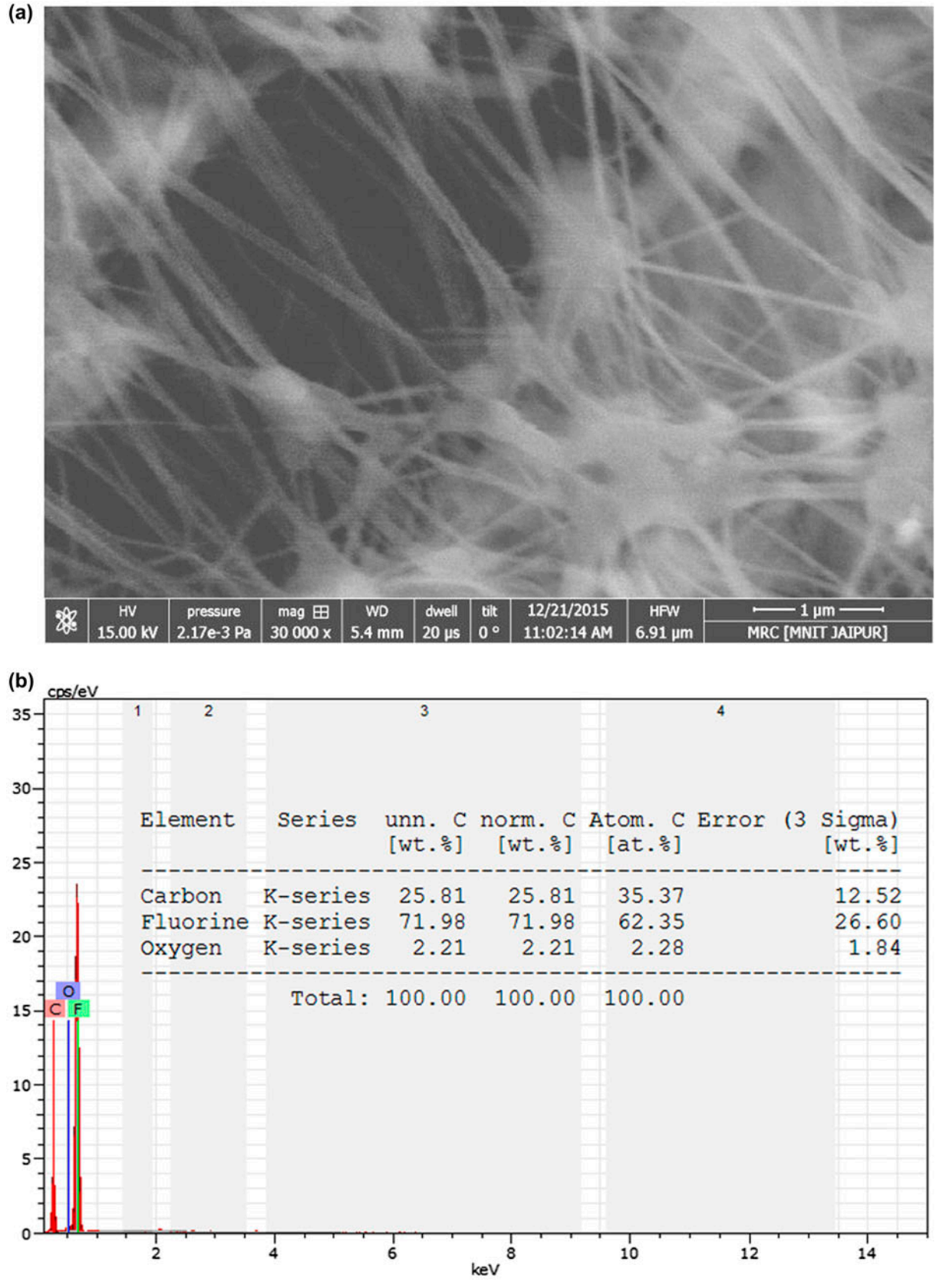


Fig. 12. (a) SEM (30,000×) micrograph and (b) EDS image of a new brand membrane.

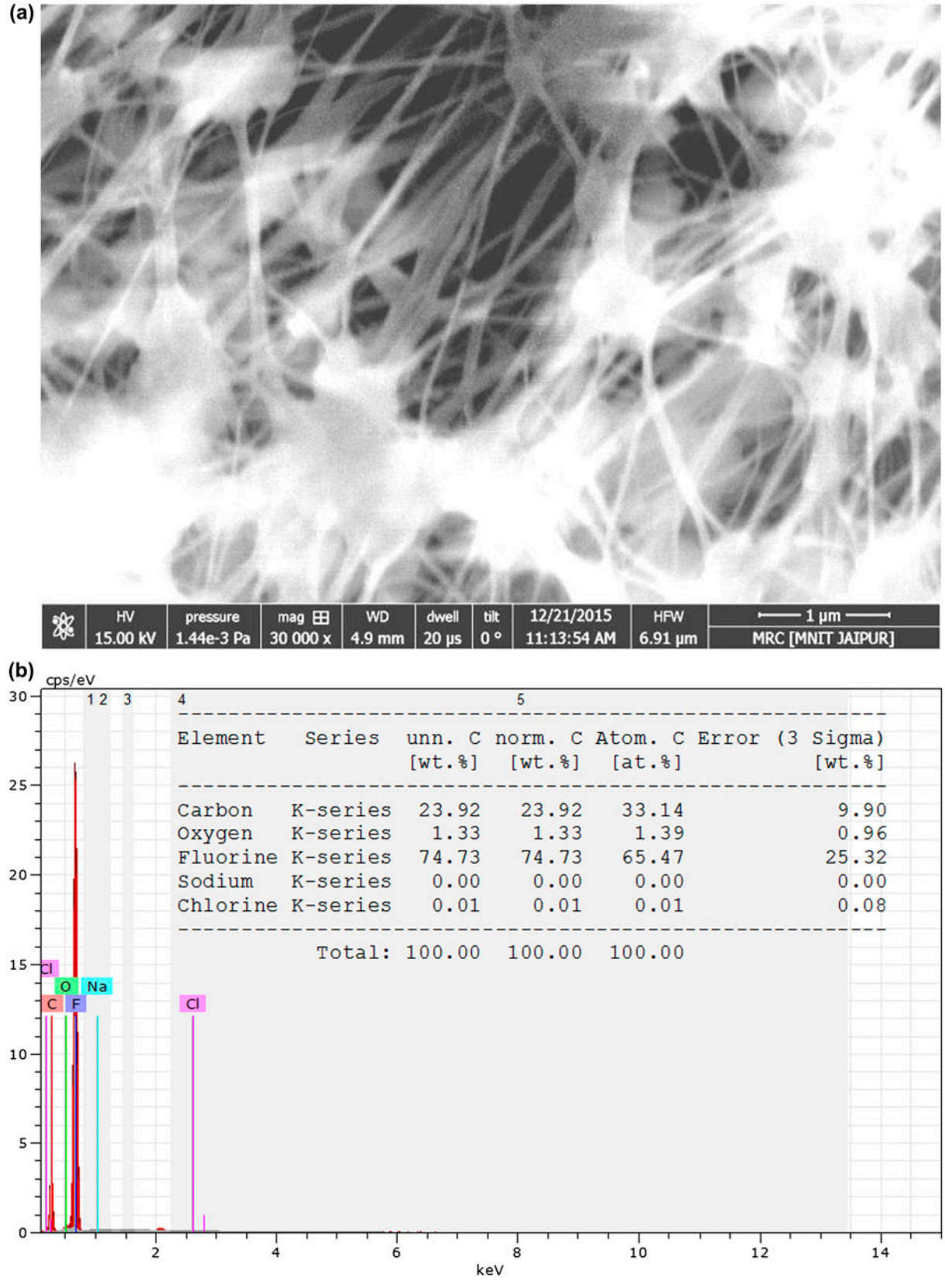


Fig. 13. (a) SEM Micrograph (30,000×) and (b) EDS image of used membrane after 180-h run time.

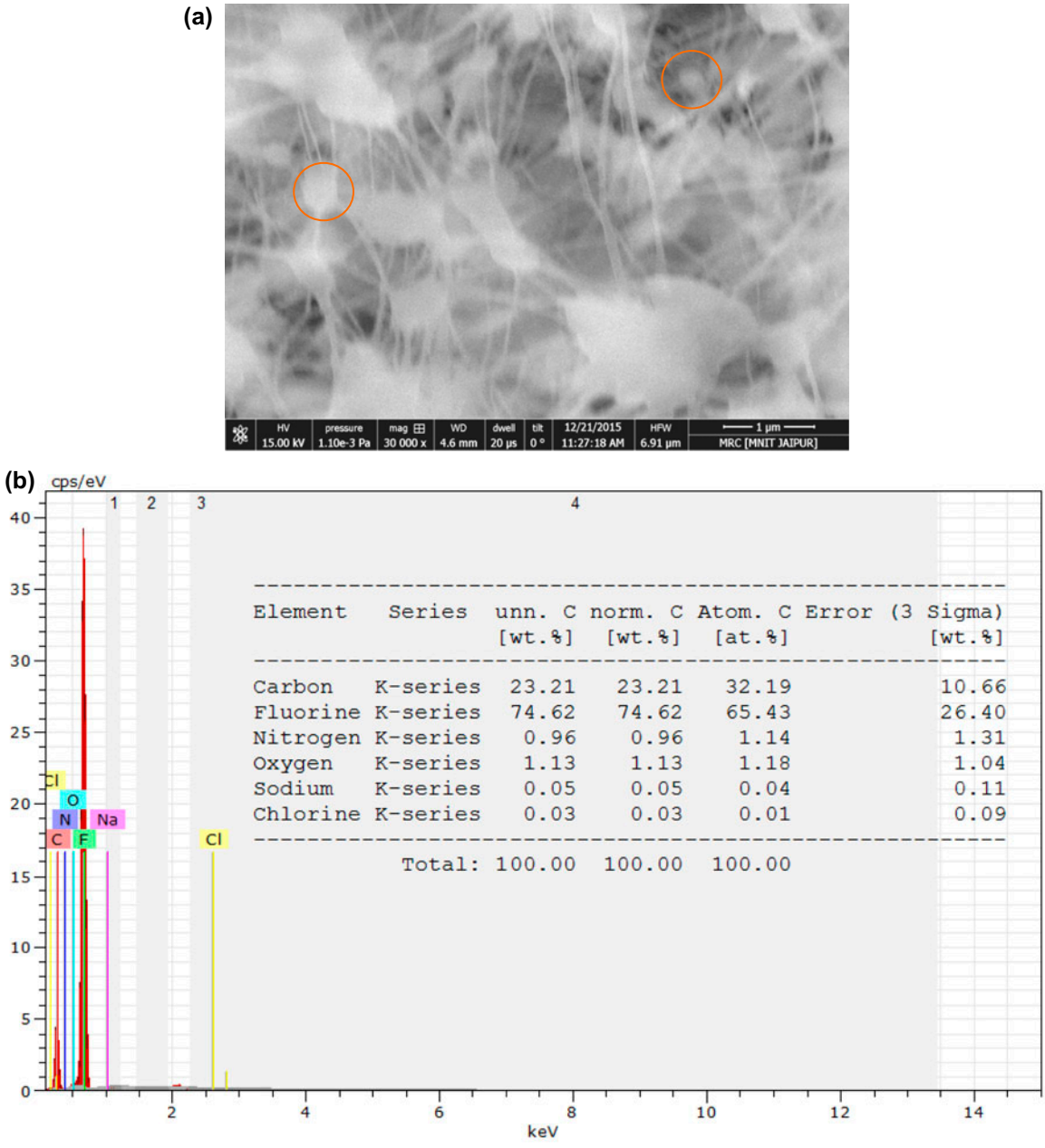


Fig. 14. (a) SEM Micrograph (30,000×), the circle represents the crystal of NaCl and (b) EDS image after 240-h run time dealing with high feed salt concentration of 40,000 ppm.

value after washing the membrane with water. In the present study, at 20 g/l of salt concentration in feed solution, the permeate flux was observed to decrease by 8% over 180 h. Mericq et al. [36] have also reported 33.6% decrease in permeate flux for synthetic sea water solution of salt concentration 300 g/l and about 10% decrease for 34 g/l of salt concentration in feed solution. In the later case, no crystal growth and scale deposit were observed in SEM micrograph. The EDS image of membrane after 180-h run time at feed salt concentration of 20,000 ppm is shown in Fig. 13(b). It is evident that sodium and chlorine are present in addition to those for pure membrane, which confirms salt deposition.

The SEM micrograph of PTFE hydrophobic membrane after its use for 240 h continuously at 7 kPa of permeate pressure, feed flow rate of 2 lpm, feed inlet temperature of 60˚C, and feed NaCl salt concentration

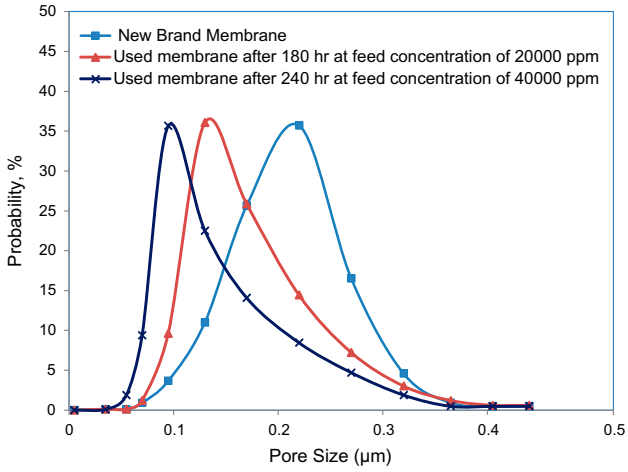


Fig. 15. Pore size distribution of PTFE membrane before and after use.

of 40 g/l is shown in Fig. 14(a). The figure shows little crystal deposition (some crystals have been encircled for clarity), which may be due to very high NaCl feed concentration on the feed side of the membrane. Also, at this high concentration, the declination of 8% in permeate flux was observed, which was supported by the SEM picture as NaCl deposit lapped only on a feeble portion of the membrane surface which increases the temperature polarization effect and reduces the membrane permeability due to salt deposition. Ultimately, the vapor pressure difference was reduced since there is reduction in partial pressure of the water vapor and significantly the declination of the permeate flux was observed in the experimental run under the above-mentioned conditions. Membrane scaling and deposition were also reported by other workers [35,37] for tap water purification. The EDS image of used membrane after 240-h run time at feed salt concentration of 40,000 ppm is shown in Fig. 14(b). It depicted the increased presence of sodium and chlorine as compared to that of 20,000 ppm salt concentration in feed and 180-h run time.

The pore size distribution estimated from software ImageJ from SEM image is given in Fig. 15. It is observed that the average pore size of a new brand membrane is 0.22 μm. However, after using for 180 and 240 h for feed concentrations of 20 and 40 g/l, respectively, the average pore size reduced due to salt deposition on the pores. Therefore, the permeate flux declined after long usage of the membrane.

## 4. Conclusions

Water recovery has been estimated from experimental data on VMD. It was found to be 86% at 183 h of operation. The developed mathematical model for recovery was in good agreement with the experimental results. Heat transfer and mass transfer correlations were developed in the range of feed flow rate of 0.5–2 lpm and feed inlet temperature of 40–60°C. The effect of salt concentration on permeate flux was also studied. Only 2% decrease in flux was observed with increase in salt concentration from 5 to 20 g/l at 60°C of feed bulk temperature. However, this declination reached 15% at feed salt NaCl concentration of 40 g/l at 60°C. Rejection of NaCl at different concentrations was observed to be more than 99%. After continuous operation upto 180 h with recycle of retentate into the feed tank, the permeate flux reduced from 26.1 to 24 kg/m$^2$ h at 60°C and feed salt concentration of 20 g/l. This 8% decline in the permeate flux was due to some salt deposition on the membrane surface. When the membrane was reused after washing with water, the permeate flux increased to 25.7 kg/m$^2$ h. The SEM and EDS images also indicated salt deposition on the membrane. The pore size distribution confirmed the cause for reduction in permeate flux after long use.

## References

[1] S. Bandini, C. Gostoli, G.C. Sarti, Separation efficiency in vacuum membrane distillation, J. Membr. Sci. 73 (1992) 217–229.
[2] D. Tong, X. Wang, M. Ali, C.Q. Lan, Y. Wang, E. Drioli, Z. Wang, Z. Cui, Preparation of Hyflon AD60/PVDF composite hollow fiber membranes for vacuum membrane distillation, Sep. Purif. Technol. 157 (2016) 1–8.
[3] M.S. El-Bourawi, Z. Ding, R. Ma, M. Khayet, A framework for better understanding membrane distillation separation process, J. Membr. Sci. 285 (2006) 4–29.
[4] G.W. Meindersma, C.M. Guijt, A.B. de Haan, Desalination and water recycling by air gap membrane distillation, Desalination 187 (2006) 291–301.
[5] V. Calabro, B.L. Jiao, E. Drioli, Theoretical and experimental study on membrane distillation in the concentration of orange juice, Ind. Eng. Chem. Res. 33 (1994) 1803–1808.
[6] B. Li, K.K. Sirkar, Novel membrane and device for vacuum membrane distillation-based desalination process, J. Membr. Sci. 257 (2005) 60–75.
[7] A.M. Alklaibi, N. Lior, Membrane-distillation desalination: Status and potential, Desalination 171 (2005) 111–131.
[8] F.A. Banat, J. Simandl, Theoretical and experimental study in membrane distillation, Desalination 95 (1994) 39–52.
[9] S. Bandini, G.C. Sarti, Heat and mass transport resistances in vacuum membrane distillation per drop, AIChE J. 45 (1999) 1422–1433.
[10] M.N. Chernyshov, G.W. Meindersma, A.B. de Haan, Modelling temperature and salt concentration distribution in membrane distillation feed channel, Desalination 157 (2003) 315–324.

[11] Z. Ding, R. Ma, A.G. Fane, A new model for mass transfer in direct contact membrane distillation, Desalination 151 (2003) 217–227.
[12] F.A. Banat, J. Simandl, Desalination by membrane distillation: A parametric study, Sep. Sci. Technol. 33 (1998) 201–226.
[13] P.J. Foster, A. Burgoyne, M.M. Vahdati, Improved process topology for membrane distillation, Sep. Purif. Technol. 21 (2001) 205–217.
[14] M. Gryta, M. Tomaszewska, Heat transport in the membrane distillation process, J. Membr. Sci. 144 (1998) 211–222.
[15] M. Gryta, M. Tomaszewska, A.W. Morawski, Membrane distillation with laminar flow, Sep. Purif. Technol. 11 (1997) 93–101.
[16] M. Khayet, P. Godino, J.I. Mengual, Theory and experiments on sweeping gas membrane distillation, J. Membr. Sci. 165 (2000) 261–272.
[17] M. Khayet, T. Matsuura, Pervaporation and vacuum membrane distillation processes: Modeling and experiments, AIChE J. 50 (2004) 1697–1712.
[18] K.W. Lawson, D.R. Lloyd, Membrane distillation. II. Direct contact MD, J. Membr. Sci. 120 (1996) 123–133.
[19] L. Martinez-Diez, F.J. Florido-Diaz, A. Hernandez, P. Pradanos, Characterization of three hydrophobic porous membranes used in membrane distillation, J. Membr. Sci. 203 (2002) 15–27.
[20] L. Martinez-Diez, M.I. Vázquez-González, Temperature and concentration polarization in membrane distillation of aqueous salt solutions, J. Membr. Sci. 156 (1999) 265–273.
[21] J.I. Mengual, M. Khayet, M.P. Godino, Heat and mass transfer in vacuum membrane distillation, Int. J. Heat Mass Transfer 47 (2004) 865–875.
[22] J. Phattaranawik, R. Jiraratananon, A.G. Fane, Heat transport and membrane distillation coefficients in direct contact membrane distillation, J. Membr. Sci. 212 (2003) 177–193.
[23] S. Upadhyaya, K. Singh, S.P. Chaurasia, R.K. Dohare, M. Agarwal, Mathematical and CFD modeling of vacuum membrane distillation for desalination, Desalin. Water Treat. (2015) 1–16.
[24] K.W. Lawson, D.R. Lloyd, Membrane distillation, J. Membr. Sci. 124 (1997) 1–25.
[25] F. Banat, F.A. Al-Rub, K. Bani-Melhem, Desalination by vacuum membrane distillation: Sensitivity analysis, Sep. Purif. Technol. 33 (2003) 75–87.
[26] S. Bandini, A. Saavedra, G.C. Sarti, Vacuum membrane distillation: Experiments and modeling, AIChE J. 43 (1997) 398–408.
[27] S. Bouguecha, R. Chouikh, M. Dhahbi, Numerical study of the coupled heat and mass transfer in membrane distillation, Desalination 152 (2003) 245–252.
[28] M.A. Izquierdo-Gil, G. Jonsson, Factors affecting flux and ethanol separation performance in vacuum membrane distillation (VMD), J. Membr. Sci. 214 (2003) 113–130.
[29] B.L. Pangarkar, S.B. Parjane, R.M. Abhang, M. Guddad, The heat and mass transfer phenomena in vacuum membrane distillation for desalination, Int. J. Chem. Biomol. Eng. 3 (2010) 33–38.
[30] Z. Xu, Y. Pan, Y. Yu, CFD simulation on membrane distillation of NaCl solution, Front. Chem. Eng. China 3 (2009) 293–297.
[31] M. Khayet, T. Matsuura, Preparation and characterization of polyvinylidene fluoride membranes for membrane distillation, Ind. Eng. Chem. Res. 40 (2001) 5710–5718.
[32] M. Khayet, T. Matsuura, Application of surface modifying macromolecules for the preparation of membranes for membrane distillation, Desalination 158 (2003) 51–56.
[33] K.W. Lawson, D.R. Lloyd, Membrane distillation. I. Module design and performance evaluation using vacuum membrane distillation, J. Membr. Sci. 120 (1996) 111–121.
[34] T. Mohammadi, M.A. Safavi, Application of Taguchi method in optimization of desalination by vacuum membrane distillation, Desalination 249 (2009) 83–89.
[35] K. Karakulski, M. Gryta, A. Morawski, Membrane processes used for potable water quality improvement, Desalination 145 (2002) 315–319.
[36] J.P. Mericq, S. Laborie, C. Cabassud, Vacuum membrane distillation for an integrated seawater desalination process, Desalin. Water Treat. 9 (2009) 287–296.
[37] M. Gryta, Application of membrane distillation process for tap water purification, Membr. Water Treat. 1 (2010) 1–12.